



HAL
open science

Diffusive impurity transport driven by trapped particle turbulence in tokamak plasmas

Etienne Gravier, Maxime Lesur, X. Garbet, Y. Sarazin, J. Médina, K. Lim,
M. Idouakass

► **To cite this version:**

Etienne Gravier, Maxime Lesur, X. Garbet, Y. Sarazin, J. Médina, et al.. Diffusive impurity transport driven by trapped particle turbulence in tokamak plasmas. *Physics of Plasmas*, 2019, 26 (8), pp.082306. 10.1063/1.5107443 . hal-02275470

HAL Id: hal-02275470

<https://hal.science/hal-02275470>

Submitted on 8 Feb 2023

HAL is a multi-disciplinary open access archive for the deposit and dissemination of scientific research documents, whether they are published or not. The documents may come from teaching and research institutions in France or abroad, or from public or private research centers.

L'archive ouverte pluridisciplinaire **HAL**, est destinée au dépôt et à la diffusion de documents scientifiques de niveau recherche, publiés ou non, émanant des établissements d'enseignement et de recherche français ou étrangers, des laboratoires publics ou privés.

Diffusive impurity transport driven by trapped particle turbulence in tokamak plasmas

E. Gravier¹, M. Lesur¹, X. Garbet², Y. Sarazin²,
J. Médina¹, K. Lim¹, M. Idouakass¹

¹IJL, UMR 7198 CNRS - Université de Lorraine, 54 000 Nancy, France

²CEA, IRFM, 13 108 Saint-Paul-lez-Durance, France

Abstract

The diffusive impurity transport as a function of the charge and mass numbers is investigated in an ion driven or an electron driven turbulence, in the limit of zero impurity temperature gradient. It is found that the impurity transport decreases slightly with increasing mass number, and depends much strongly on the charge number. Moreover, this transport depends on the nature of the instability that drives turbulence. The impurity flux due to Trapped Electron Mode (TEM) turbulence increases with the charge number Z . In contrast, it is found to decrease with Z in the Trapped Ion Mode (TIM) dominated. In order to explain these observations, the quasilinear flux is derived and is compared with results obtained from the nonlinear simulations. Quasi-linear theory qualitatively reproduces the gyro-kinetic numerical observations.

I. INTRODUCTION AND MODEL

In tokamak plasmas, all particles that are not electrons or do not contribute to the reaction of fusion are defined as impurities. For instance argon or neon can be introduced in the plasma edge as impurity seeding used for tailoring the radiation profile near the plasma-facing components. The propagation of these particles into the plasma core can be problematic. Moreover, transport and accumulation of tungsten from the wall to the core can also be prohibitive, for concentrations as low as 3×10^{-5} [1]. In contrast helium ash produced by the reactions of fusion must be transported from the core to the wall. Therefore impurity accumulation in the plasma core must be avoided and impurity transport is an issue that needs to be understood. For example, the direction of this transport, i.e. inwards or

outwards, can be predicted by neoclassical theory, depending on both main ion density gradient and temperature gradient. In addition, turbulence also contributes to impurity flux.

In this work, we focus on turbulence issues. The thermodiffusive pinch and the curvature-driven pinch, respectively second and third terms on the RHS in Eq.(1),

$$\Gamma = -D \frac{\partial n}{\partial r} + C_T \frac{\partial T}{\partial r} + C_P \quad (1)$$

are neglected in our calculations, so that impurity transport Γ calculations only include diffusive transport (first term on the RHS of Eq.1, $\Gamma = -D \frac{\partial n}{\partial r}$). Moreover, our model is collisionless, meaning that neoclassical transport is not taken into account. The expected increasing importance of the turbulent transport of impurities in a reactor plasma motivates our study. Turbulent impurity transport is expected to have a larger weight in future reactor size plasmas than in present devices [2], in which neoclassical transport is relatively higher. Isotopic effects (hydrogenic mass effects) on impurity transport have been studied [3], but these investigations are limited to $Z = 2 - 3$, whereas we aim at covering a larger range. The dependence of impurity transport on the impurity species have been studied as well [2, 4–13], but without decoupling the impacts of Z and A , or focusing on the peaking factor. In a previous paper [14], we have shown how a large concentration of tungsten can change the nature of the turbulence in the case of active species. In the present article we perform scalings for the impurity diffusion coefficients with the impurity charge and the mass numbers, and with the TEM or TIM driven modes, in the case where impurity concentrations do not affect the nature of the turbulence. Impurity turbulent fluxes are investigated via both gyro-bounce-kinetic simulations and quasi-linear theory. The gyrokinetic code we use is named TERESA (Trapped Element REduction in Semi lagrangian Approach) [15]. It should be noted that the results of nonlinear simulations are often compared with the quasi-linear theory, which is relevant because its estimations of turbulent fluxes in most cases remain in good agreement with nonlinear gyrokinetic simulations [16] as well as with experimental results [17], despite crude simplifications, and even if in some cases discrepancies between nonlinear simulations and quasi-linear predictions are observed [2].

To complete this introduction and for the benefit of the reader, we summarize below the main assumptions and equations of the gyrokinetic model [14] needed to understand the new investigations and results described in the rest of the article. The reader can find further information in the references [14, 15, 18–28].

The model is relevant for relatively low frequency modes, such as Trapped-Ion Modes (TIM) and Trapped-Electron Modes (TEM). TEM and TIM are instabilities that are characterized by frequencies ω of the order of ω_d , the precession frequency. And this latter frequency is smaller than ω_b , the bounce frequency, which itself is smaller than the cyclotron frequency ω_c . Therefore it is possible to gyro-average and bounce-average the Vlasov equation, thus filtering out the fast cyclotron and bounce frequencies, and the small space scales ρ_c (gyro-radius) and δ_b (banana width). These assumptions lead to a reduction of dimensionality, from 5D gyro kinetics, to 4D gyrobounce-gyrokinetics. We consider an adiabatic response of the passing particles, thus our reduced model with trapped kinetic particles covers both TIM/TEM regimes simultaneously but precludes other instabilities such as Ion-Temperature-Gradient (ITG) or Electron-Temperature-Gradient (ETG) instabilities.

The Vlasov equation reads:

$$\frac{\partial f_s}{\partial t} - [\mathcal{J}_{0,s}\phi, f_s]_{\alpha,\psi} + \frac{\Omega_d E}{Z_s} \frac{\partial f_s}{\partial \alpha} = 0 \quad (2)$$

f_s is the gyro-bounce-averaged particle distribution function. The subscript $s = i, e, z$ stands for the species considered (main ion, electron, or impurity), and ϕ is the plasma potential. E is the particle kinetic energy. $\alpha = \varphi - q\theta$, with φ the toroidal angle, θ the poloidal angle, and q the safety factor. ψ is the magnetic flux, function of the radius: $\psi = 1$ stands for the core plasma and $\psi = 0$ for the plasma edge. Z_s is the charge number. $\Omega_d = \frac{Z_s \omega_{d,s}}{E}$, with $\omega_{d,s}$ the toroidal precession frequency for the species s [29]. For the main ion species, we choose $\Omega_d = 1$, and we neglect the variation of Ω_d over the radius (Ω_d only depends on the sign of the charge).

The gyro-bounce-averaging operator writes:

$$\mathcal{J}_{0,s} = \left(1 - \frac{E}{T_{0,s}} \frac{\delta_{b0,s}^2}{4} \partial_\psi^2\right)^{-1} \left(1 - \frac{E}{T_{0,s}} \frac{q^2 \rho_{c0,s}^2}{4a^2} \partial_\alpha^2\right)^{-1} \quad (3)$$

where $\rho_{c0,s}$ and $\delta_{b0,s}$ are the Larmor radius and the banana width (expressed in units of ψ), $T_{0,s}$ is the equilibrium temperature at $\psi = 0$, normalized to an arbitrary reference temperature T_0 . $\omega_0 = T_0/(eR_0^2 B_\theta)$ corresponds to the ion precession frequency at the reference temperature T_0 (time is normalized to ω_0), and $L_\psi = aR_0 B_\theta$ is the radial length of the simulation box in units of ψ . ψ is normalized to L_ψ .

The normalized quasi-neutrality constraint writes:

$$\frac{2}{\sqrt{\pi}} \sum_s \left(Z_s \mathcal{C}_s \int_0^\infty \mathcal{J}_{0,s} f_s E^{1/2} dE \right) = C_{ad} (\phi - \varepsilon_\phi < \phi >_\alpha) - C_{pol} \sum_s \mathcal{C}_s \tau_s Z_s^2 \Delta_s \phi \quad (4)$$

with $\mathcal{C}_s = n_s/n_{0,e}$ the concentration of the species s (n_s is the population density, $n_{0,e}$ the electron density at equilibrium), $C_{pol} = e\omega_0 L_\psi / T_0$, $C_{ad} = C_{pol} \frac{1-f_T}{f_T} \sum_s (Z_s^2 \mathcal{C}_s \tau_s)$ where f_T is the fraction of trapped particles and $\tau_s = T_0/T_{0,s}$. The Laplacian operator expresses the difference between the particle density and the gyro-bounce-center density, corresponding to an effective polarization. ε_ϕ is a control parameter which governs the response of the adiabatic passing particles. Regarding this response, the reader can find further information in the references [14, 25, 30]. Hereafter, only the case $\varepsilon_\phi = 0.3$ is considered.

In section II, linear results and nonlinear simulations are presented. It is shown how impurities behave as a function of the mass and charge numbers. In section III, the quasi-linear impurity fluxes are derived and compared with nonlinear numerical results. Finally, a brief summary of the results along with a conclusion are given in section IV.

II. IMPURITY TRANSPORT AS A FUNCTION OF THE CHARGE NUMBER AND THE MASS NUMBER

We choose to implement the equilibrium distribution function as follows:

$$F_{eq,s} = \frac{n_{0,s}}{T_{0,s}^{3/2}} \exp\left(-\frac{E}{T_{0,s}}\right) \left[1 + \left(\kappa_{n,s} + \left(\frac{E}{T_{0,s}} - \frac{3}{2} \right) \kappa_{T,s} \right) \psi \right] \quad (5)$$

For electrons and main ions, $\kappa_{T,ei} = \frac{1}{T_{e,i}} \partial_\psi T_{e,i}$ have finite values. For impurities, we choose $\kappa_{T,Z} = 0$ so that no thermodiffusion will appear for impurity transport. $\kappa_{n,s}$ is defined as $\frac{1}{n_s} \partial_\psi n_s$. The curvature driven pinch is also neglected in this model, since a Taylor expansion at $\psi = 0$ of a Maxwellian distribution yields

$$F_{eq,s}^* = F_{eq,s} - \frac{n_{0,s}}{T_{0,s}^{3/2}} \frac{e\Omega_d E}{T_{0,s}} \psi \exp\left(-\frac{E}{T_{0,s}}\right) \quad (6)$$

The latter term is responsible for curvature-driven pinch, and is neglected in Eq.5. Therefore, impurity transport calculations only include diffusive transport. The transport across the magnetic field is therefore adequately characterized as diffusivity.

For the linear study, we use the linear dispersion derived in [14]. It reads:

$$D = 0 = C_n - \sum_s Z_s \mathcal{C}_s \tau_s \int_0^\infty J_{n,s}^2 \frac{\kappa_{n,s} + \kappa_{T,s}(\xi_s - \frac{3}{2})}{\frac{\Omega_d}{Z_s}(\xi_s - W_s)} e^{-\xi_s} \xi_s^{\frac{1}{2}} d\xi \quad (7)$$

with

$$C_n = \frac{\sqrt{\pi}}{2} \left[C_{ad} + C_{pol} n^2 \sum_s \mathcal{C}_s \tau_s Z_s^2 \rho_{c0,s}^2 + C_{pol} k^2 \sum_s \mathcal{C}_s \tau_s Z_s^2 \delta_{b0,s}^2 \right] \quad (8)$$

Here, $\xi = \frac{E}{T_{0,s}}$, $W_s = \frac{Z_s \omega}{n \Omega_d T_{0,s}}$, n being the mode number in the α -direction, $k = \pi$ the most unstable radial mode and ω the complex mode frequency. This dispersion relation will be solved to find the growth rates and real frequencies of the TEM and TIM instabilities for two different cases we investigate in this paper. For linearly solving Eq.(7), we scan the (ω_r, ω_i) plane, searching for values of ω such that the RHS of Eq.(7) vanishes within machine precision. For this purpose a method that finds the minimum of a scalar function of several variables, starting at an initial state, and uses the simplex search method [31], is used. Actually we start the scan from several initial values in the (ω_r, ω_i) plane in order to get all the possible roots. Among these solutions one finds the couple (ω_r, ω_i) for which the instability growth rate ω_i is maximum. We simultaneously look at the region where ω_r is negative (TEM instability) and the region where ω_r is positive (TIM instability). We retain the maximum of ω_i for each of the two regions.

\mathcal{C}_D	\mathcal{C}_e	\mathcal{C}_Z	$\kappa_{n,D}$	$\kappa_{n,e}$	$\kappa_{n,Z}$	$\frac{T_{0,D,Z}}{T_{0,e}}$
0.9964	1.0	10^{-5}	0.1	0.099604	-1	1.0

TABLE I: Main parameters used for the linear study and nonlinear simulations. The subscripts D , e and Z stand for deuterium, electron and impurities, respectively.

$\rho_{c,D}$	$\rho_{c,e}$	$\rho_{c,Z=2}$	$\rho_{c,Z=4}$	$\rho_{c,Z=8}$	$\rho_{c,Z=10}$	$\rho_{c,Z=12}$
6×10^{-3}	10^{-4}	9.49×10^{-3}	4.74×10^{-3}	2.38×10^{-3}	1.90×10^{-3}	1.58×10^{-3}

TABLE II: Larmor radii used for the linear study and nonlinear simulations, for deuterium (D), electrons (e) and impurities (Z). The values of the Larmor radii are at the thermal velocity and the approximation of constant orbit widths is used.

$\delta_{b,D}$	$\delta_{b,e}$	$\delta_{b,Z=2}$	$\delta_{b,Z=4}$	$\delta_{b,Z=8}$	$\delta_{b,Z=10}$	$\delta_{b,Z=12}$
6×10^{-2}	10^{-3}	9.49×10^{-2}	4.74×10^{-2}	2.37×10^{-2}	1.90×10^{-2}	1.58×10^{-2}

TABLE III: Banana widths used for the linear study and nonlinear simulations, for deuterium (D), electrons (e) and impurities (Z). The values of the banana widths are at the thermal velocity and the approximation of constant orbit widths is used.

Here and in the remainder of the paper, we consider a plasma composed of deuterium as the main ion species, electrons and impurity species. In our calculations and simulations, all species are considered as active species, meaning that each species is described by its own distribution function, and each species is taken into account in the quasi-neutrality constraint.

We choose five different simulated impurities with the same mass number ($A = 20$) but with 5 different charge numbers $Z = 2, 4, 8, 10$ and 12 . Regarding the A -dependence, another set of simulations is considered with the same charge number ($Z = 4$) but with 5 different mass numbers $A = 10, 30, 50, 70$ and 90 in order to cover the same \sqrt{A}/Z range as in the case of the Z -dependence. Other parameters used as inputs for the linear code and the nonlinear code are given Tab.I, Tab.II and Tab.III. Species concentrations and density gradients are chosen according to quasi-neutrality, assuming that $n_{0,e} = 1$, $\kappa_{n,D} = 0.1$, $\mathcal{C}_Z = 10^{-5}$ and $\kappa_{n,Z} = -10^{-5}$ for all impurities. The minus sign for $\kappa_{n,Z}$ means that the impurity density is larger at the plasma edge than at the plasma core, according to the fact that main impurities come from the wall. It should be noted that the results presented hereafter do not depend on the sign of $\kappa_{n,Z}$, and the plus sign could have been chosen. Other quantities from Tab.I are evaluated according to quasi-neutrality:

$$\sum_s Z_s \mathcal{C}_s = 0 \quad (9)$$

which also leads to a constraint on $\kappa_{n,s}$:

$$\sum_s Z_s \mathcal{C}_s \kappa_{n,s} = 0 \quad (10)$$

The two different cases investigated in this paper are now presented.

The first one corresponds to $\partial_\psi T_D = 0.135$ and $\partial_\psi T_e = 0.18$. The dispersion relation

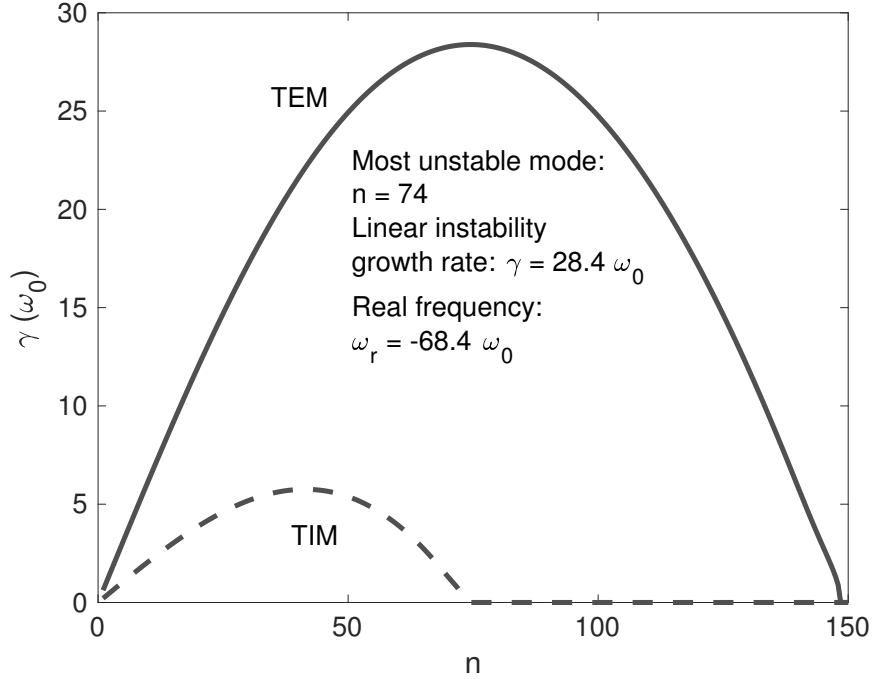


FIG. 1: Instability growth rates plotted against the mode number n , in the case $\partial_\psi T_e = 0.18$ and $\partial_\psi T_D = 0.135$, for TEM (solid line) and TIM (dotted line). For these temperature gradients the most unstable mode $n = 74$ is a trapped electron mode (TEM).

(Eq.7) is numerically solved and TEM are found to be more unstable than TIM. This case is referred to as the TEM case (Fig.1). For these temperature gradients the most unstable mode is $n = 74$, the instability growth rate is $\gamma = 28.4 \omega_0$, and the real frequency $\omega_r = -68.4 \omega_0$. In this case and with the ITER parameters, it should be noted that the order of magnitude of ω_r/ω_b is about 0.2 for deuterium, and 0.005 for electrons. Thus, even if ω_r is much less than ω_b in the case of electrons, for deuterium ions the condition of the mode frequency lower than the bounce frequency is less safely met. Nevertheless, with different electron/ion mass ratios leading to lower modes and smaller ω_r/ω_b , the results and the trends presented hereafter are very similar.

For the second case, $\partial_\psi T_D = 0.18$ and $\partial_\psi T_e = 0.135$. The dispersion relation is numerically solved and TIM are found to be more unstable than TEM. This case will be referred to as the TIM case (Fig.2). For these temperature gradients the most unstable mode is $n = 60$, the instability growth rate is $\gamma = 23.4 \omega_0$, and the real frequency $\omega_r = 56.9 \omega_0$.

The results of the nonlinear simulations are now presented. A semi-lagrangian method for the numerical resolution of the Vlasov equation is used [32]. These simulations have

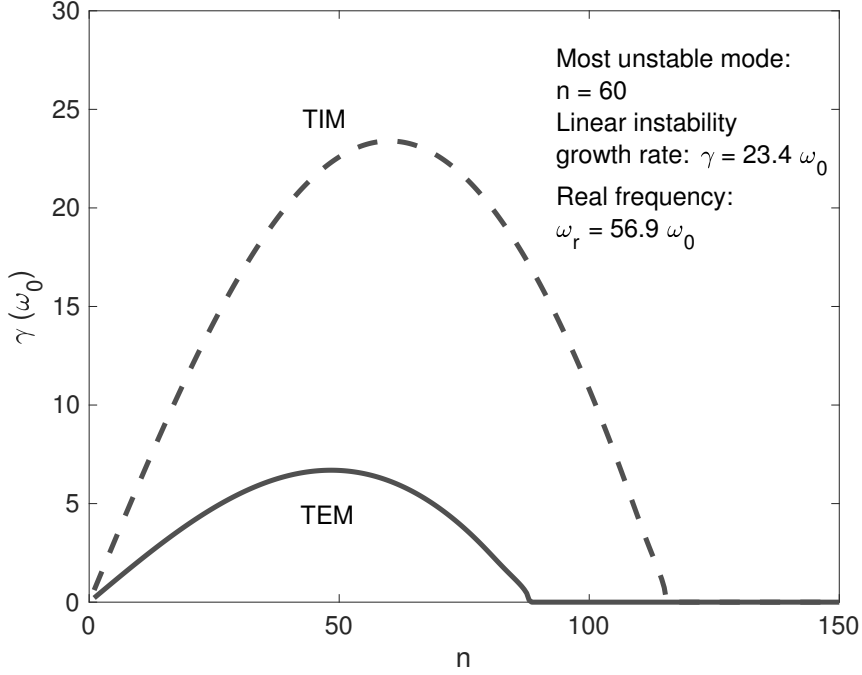


FIG. 2: Instability growth rates plotted against the mode number n , in the case $\partial_\psi T_e = 0.135$ and $\partial_\psi T_D = 0.18$, for TEM (solid line) and TIM (dotted line). For these temperature gradients the most unstable mode $n = 60$ is a trapped ion mode (TIM).

been performed with $N_\psi = 256$, $N_\alpha = 1024$, $N_E = 192$. The numerical simulations are done using a thermal and density bath as boundary conditions: the temperature and density are fixed at $\psi = 0$ and $\psi = 1$. Dirichlet boundary conditions are imposed on the potential. The simulation parameters correspond to a radial box size of 166 Deuterium Larmor radii. First we noticed (not shown in this paper) that for both cases the most unstable modes displayed by the nonlinear TERESA simulations in the linear phase correspond to the linear growth rates given by the linear analysis, as well as the direction of propagation, along the α -direction for TIM instabilities and in the opposite direction for TEM instabilities. Then in the nonlinear state the fastest growing modes couple to the other eigenmodes, driving them up to the saturation level.

In order to evaluate impurity transport, while smoothing out fast turbulent fluctuations, we plot the cumulative flux along the ψ -direction (meaning along the radial direction) given by:

$$\Gamma_{cumul} = \int_0^t \Gamma(t^*) dt^* \quad (11)$$

with [21]:

$$\Gamma(t) = -\frac{2}{\sqrt{\pi}} \int_0^{2\pi} d\alpha \int_0^\infty f \partial_\alpha (\mathcal{J}\phi) E^{1/2} dE \quad (12)$$

A. Trapped electron mode case

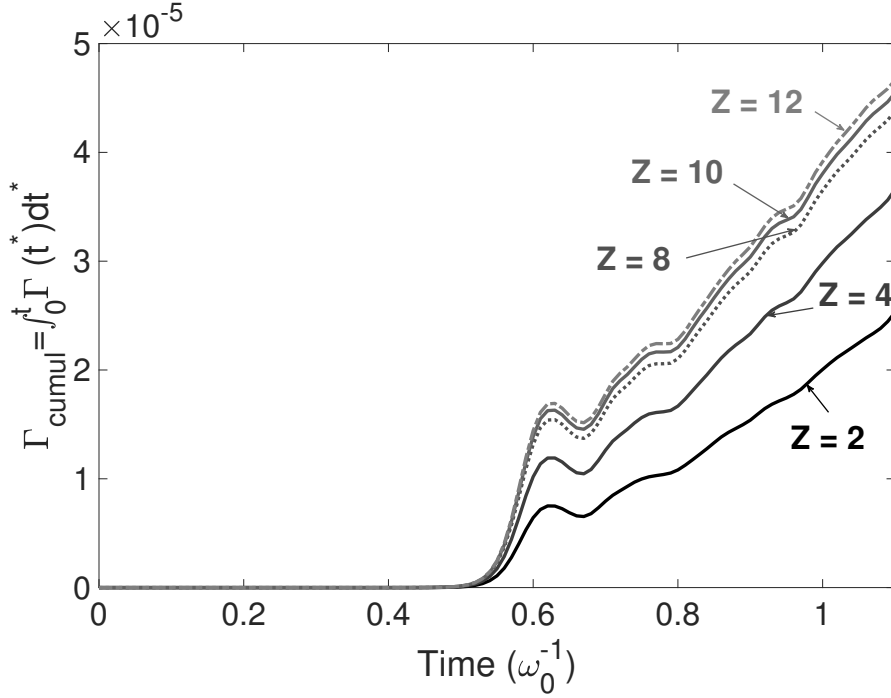


FIG. 3: Impurity cumulative flux $\int_0^t \Gamma(t^*) dt^*$ plotted against time in the case of a TEM turbulence. Different charge numbers are considered, with the same mass number $A = 20$.

The higher charge impurity has larger impurity flux.

We focus on the TEM case. The results regarding the Z -dependence are presented in Fig.3. First a linear phase is observed, followed by the saturation phase, at about $t = 0.6 \omega_0^{-1}$. The system reaches a nearly steady state from $t = 0.8 \omega_0^{-1}$. Then the cumulative flux increases almost linearly, meaning that impurity particle flux is nearly constant. The slopes are determined from $t = 0.8$ to $t = 1.1 \omega_0^{-1}$, and we can then evaluate the impurity flux Γ_Z . As we assume a pure diffusive transport, the global diffusion coefficient is given by:

$$D_Z = -\frac{\Gamma_Z}{\partial_\psi n_Z} \quad (13)$$

The diffusion coefficients for the TEM case are presented in Fig.4. The diffusion coefficient D_{TEM} is plotted against the impurity charge number Z . The error bars correspond to the

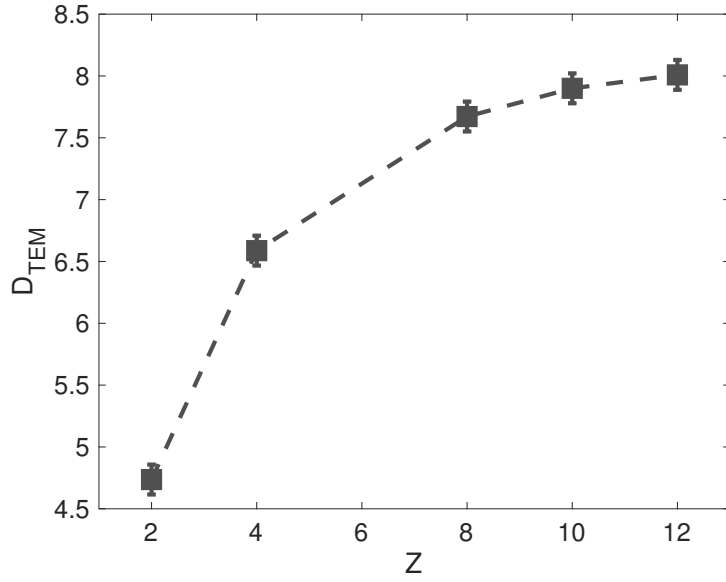


FIG. 4: Impurity diffusion D_{TEM} coefficient plotted against the impurity charge number Z in the case of TEM turbulence. The mass number is $A = 20$. The coefficient is calculated from Fig. 3, for $0.8 < t < 1.1$. The higher charge impurity has larger diffusion coefficient.

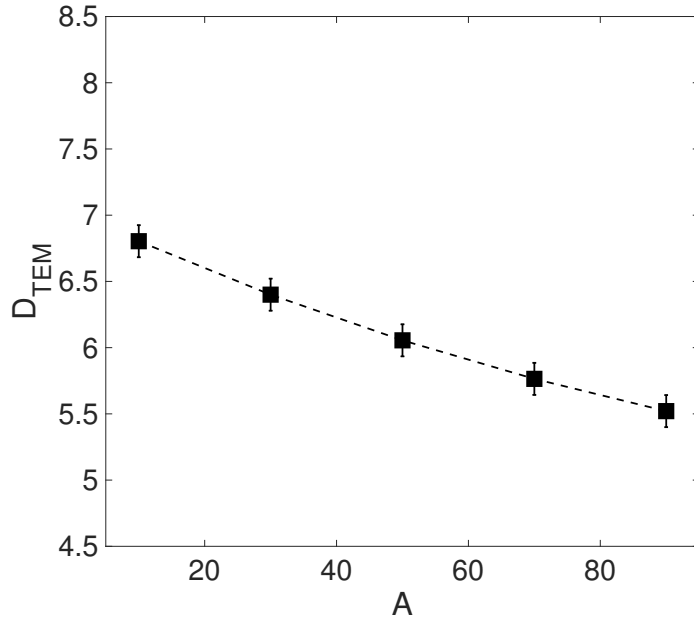


FIG. 5: Impurity diffusion D_{TEM} coefficient plotted against the mass number A in the case of TEM turbulence. The charge number is $Z = 4$. The coefficient depends more weakly on A than on Z (about 60%, the same scale as in Fig.5 is used in ordinate in order to compare both results).

uncertainty in the determination of the slopes from Fig.3. We observe in that case that the diffusion coefficient increases with the charge number. It should be noted that this trend is always observed when TEM are the main instabilities, and even if parameters are very different, for instance if we choose Larmor radii and banana widths such that the main unstable modes are much smaller (about $n = 10$ for instance). Moreover, other simulations have been performed with ε_ϕ greater than 0.3. In that case zonal flows are stronger. The diffusion coefficient still increases with the charge number, but the diffusion coefficients are smaller, as expected when zonal flows are stronger (zonal flows are structures perpendicular to the radial direction that improve plasma confinement).

Nevertheless, we observe that impurity transport becomes roughly independent of impurity charge at high impurity charges, as observed in other studies [2].

Finally, an other important result is that this transport depends weakly on the mass number A of the species. Additional simulations have been carried out for five impurities with Z constant and different values of A . We performed simulations with $Z = 4$, and $A = 10, 30, 50, 70, 90$ in order to cover approximatively the same domain in \sqrt{A}/Z as for the study of the Z -dependence (Fig.5). The variation in A of the impurity diffusion coefficient is about 60% smaller than that of in Z , for the same \sqrt{A}/Z range, and is found to decrease with A .

B. Trapped ion mode case

Then we consider the TIM case. The results regarding the Z -dependence are presented in Fig.6. First a linear phase is observed, followed by the saturation phase, at about $t = 0.75 \omega_0^{-1}$. The system reaches a nearly steady state from $t = 1.0 \omega_0^{-1}$. Then the cumulative flux increases linearly, meaning that impurity particle flux is almost constant. The slopes are determined from $t = 1.0$ to $t = 1.55 \omega_0^{-1}$, and then, as in the TEM case, we evaluate the impurity flux Γ_Z and the diffusion coefficients.

The diffusion coefficients D_{TIM} for the TIM case are presented in Fig.7. The diffusion coefficient D_{TIM} is plotted against the impurity charge number Z . The error bars correspond to the uncertainty in the determination of the slopes in Fig.6. We observe in that case that the diffusion coefficient decreases with the charge number. It should be noted that this trend is always observed when TIM are the main instabilities, even if plasma parameters are very different. The different scaling of the diffusion coefficient with Z will be shown in the section

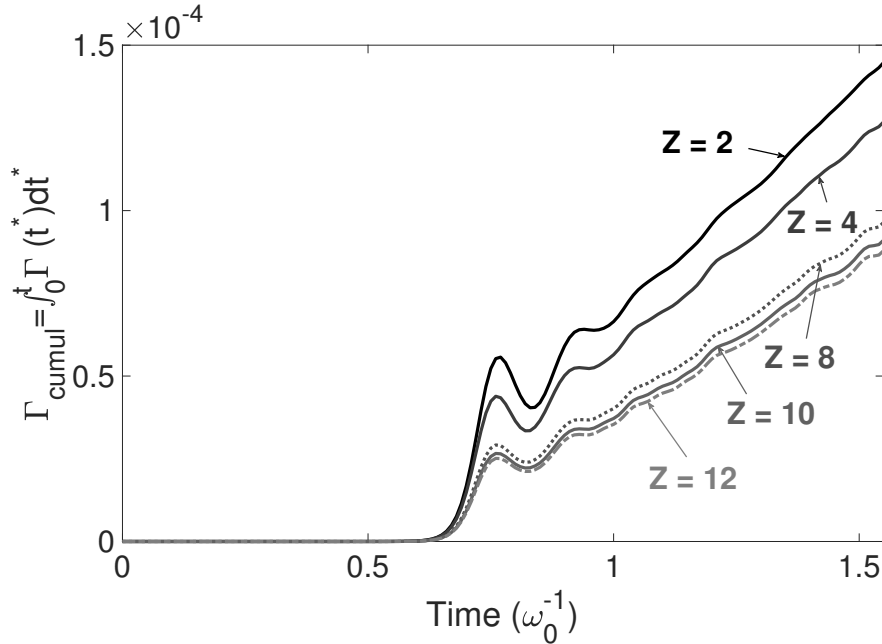


FIG. 6: Impurity cumulative flux $\int_0^t \Gamma(t^*) dt^*$ plotted against time in the case of a TIM turbulence. Different charge numbers are considered, with the same mass number $A = 20$.

The higher charge impurity has smaller impurity flux.

III to be related to a drift resonance.

Nevertheless, as in the TEM case we observe that impurity transport becomes roughly independent of impurity charge at high impurity charge numbers.

As in the TEM case, an other important result is that this transport depends weakly on the mass number A of the species. Simulations have been performed for five impurities with Z constant and different values of A . Again, we also performed simulations with $Z = 4$, and $A = 10, 30, 50, 70, 90$ in order to cover approximatively the same domain in \sqrt{A}/Z . (Fig.8). The variation in A of the impurity diffusion coefficient is about 80% smaller than that of in Z , for the same \sqrt{A}/Z range, and is found to decrease with A .

C. Conclusion of the numerical simulations

From these results we can conclude that in the case of turbulence driven by trapped particles the impurity diffusive transport depends weakly on the mass number, but depends mainly on the charge number. Moreover this transport depends on the nature of the instability that drives turbulence: the diffusion coefficient is found to increase with Z in the case of TEM turbulence, while the diffusion coefficient is found to decrease with Z in the TIM

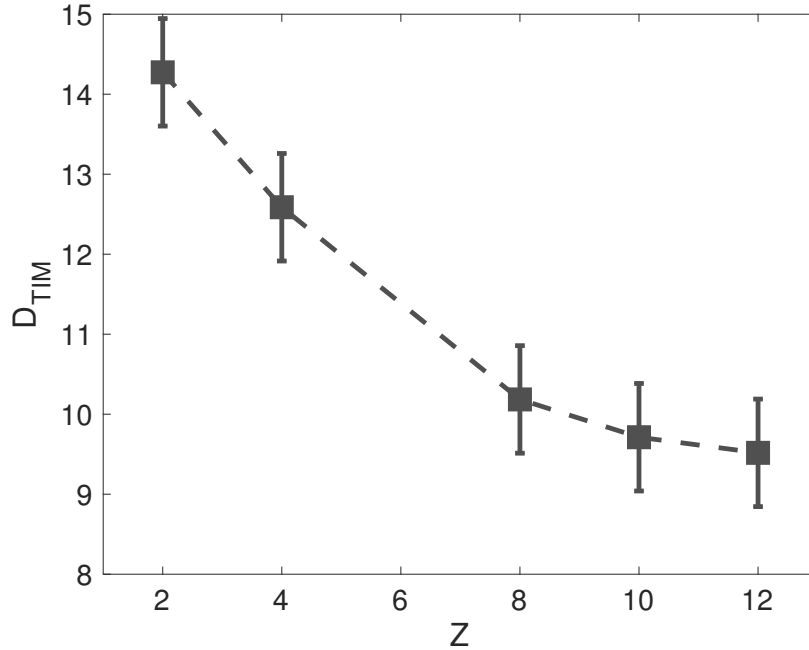


FIG. 7: Impurity diffusion coefficient D_{TIM} plotted against the impurity charge number Z in the case of TIM turbulence. The mass number is $A = 20$. The coefficient is calculated from Fig. 6, for $1.07 < t < 1.55$. The higher charge impurity has smaller diffusion coefficient.

dominated case.

We noticed that the change of flux regimes arises from the phase shifts between the density and potential fluctuations. These phase-shifts increase with Z in the case of TEM turbulence while they come down with Z in the case of TIM turbulence.

In order to explain these observations, in the next section a quasi-linear calculation of impurity transport is derived from the TERESA model and comparisons with the numerical simulations are presented.

III. COMPARISON BETWEEN NUMERICAL SIMULATIONS AND THEORETICAL PREDICTIONS

In this section, the out of phase part of the distribution function to potential fluctuations is derived from the eigenmodes, and the quasi-linear particle fluxes are determined, taking the power spectrum of the plasma potential fluctuations and the gradient parameters from TERESA simulation as input. Then the comparisons between the theoretically predicted

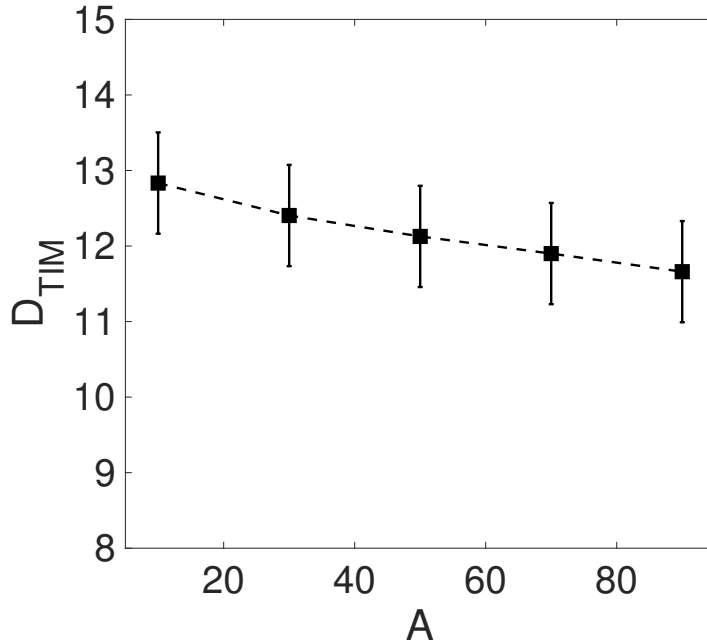


FIG. 8: Impurity diffusion D_{TIM} coefficient plotted against the mass number A in the case of TIM turbulence. The charge number is $Z = 4$. The coefficient depends more weakly on A than on Z (about 80%, the same scale as in Fig.8 is used in ordinate in order to compare both results).

impurity flux and the nonlinear impurity transport simulations are presented.

The banana-center distribution function f of one species (here we consider an impurity species and the subscript s is dropped) obeys the Vlasov equation:

$$\frac{\partial f}{\partial t} - [\mathcal{J}\phi, f] + \frac{\Omega_d E}{Z} \frac{\partial f}{\partial \alpha} = 0 \quad (14)$$

with

$$[\mathcal{J}\phi, f] = \frac{\partial \mathcal{J}\phi}{\partial \alpha} \frac{\partial f}{\partial \psi} - \frac{\partial f}{\partial \alpha} \frac{\partial \mathcal{J}\phi}{\partial \psi} \quad (15)$$

We assume that

$$f = f_0(E, t) + f_1 + f_2 + \dots \quad (16)$$

with $f_0(E, t)$ the slowly evolving background distribution that is changing due to the effects of the unstable waves, with $\frac{1}{f_0} \frac{\partial f_0}{\partial t} \ll \gamma_k$, where γ_k are the linear growth rates of the unstable waves. $f_{n \geq 1}$ are the small magnitude high frequency perturbations, of order ε^n , with $\varepsilon \ll 1$.

Quasilinear theory assumes that the amplitudes are still small enough that frequency and instantaneous growth rates of the modes are all adequately described by the linear theory.

The linear theory yields:

$$\frac{\partial f_1}{\partial t} - \frac{\partial \mathcal{J} \phi_1}{\partial \alpha} \frac{\partial f_0}{\partial \psi} + \frac{\Omega_d E}{Z} \frac{\partial f_1}{\partial \alpha} = 0 \quad (17)$$

Moreover, quantities with subscripts $n \geq 1$ are waves and therefore have spatial averages over α that vanish ($\langle . \rangle = \frac{1}{2\pi} \int_{\alpha} . d\alpha$), so that Eq. (14), combined with Eq. (17), averaged over α and neglecting terms with an order higher than 2, writes:

$$\frac{\partial f_0}{\partial t} = \frac{\partial}{\partial \psi} \left\langle f_1 \frac{\partial \mathcal{J} \phi_1}{\partial \alpha} \right\rangle \quad (18)$$

The RHS term can be explicitly calculated by expressing the perturbations as a sum over spatial Fourier modes ($\phi_1(\alpha, t) = \sum_n \phi_n e^{in\alpha} e^{-i\omega_n t}$, and the same for f_1), and by using Eq.(17) to get f_n as a function of ϕ_n , with f_n and ϕ_n the amplitudes of the mode n of the perturbation. Assuming the developed distribution function (5) with $\kappa_T = 0$ (no thermodiffusion for impurities), the relationship between f_n and ϕ_n then writes:

$$f_n = \frac{\kappa_n}{\frac{\Omega_d}{Z} E - \frac{\omega_n}{n}} F_{eq\psi=0} \mathcal{J} \phi_n \quad (19)$$

and Eq. 18 yields:

$$\frac{\partial f_0}{\partial t} - \frac{\partial}{\partial \psi} \left(\sum_n |n \mathcal{J} \phi_n|^2 \kappa_n F_{eq\psi=0} \frac{\gamma_n}{(n \frac{\Omega_d}{Z} E - \omega_{r,n})^2 + \gamma_n^2} \right) = 0 \quad (20)$$

where the sum is over linearly unstable modes only, and with $\omega_n = \omega_{r,n} + i\gamma_n$, where $\omega_{r,n}$ and γ_n are respectively the real frequency and the linear growth rate of the mode n , determined by the linear dispersion relation (Eq.7).

By integrating this last equation over energy E (the Jacobian is proportional to $E^{1/2} dE$), we obtain:

$$\frac{\partial n_0}{\partial t} + \frac{\partial \Gamma_\psi}{\partial \psi} = 0 \quad (21)$$

with Γ_ψ the impurity transport in the radial direction:

$$\Gamma_\psi = -\kappa_n \int_E \sum_n |n \mathcal{J} \phi_n|^2 \frac{\gamma_n}{(\omega_{r,n} - n \frac{\Omega_d}{Z} E)^2 + \gamma_n^2} F_{eq\psi=0} E^{1/2} dE \quad (22)$$

Both γ_n and $\omega_{r,n}$ have very weak dependency on both Z and A , since in this article only trace impurities are considered, and therefore turbulence is governed by electrons and main ions: The more direct impacts of impurity species in Poisson equation are negligible for $Z_s^2 \mathcal{C}_s \ll 1$ [33]. Therefore, from this last equation (22) we can see that the radial impurity flux depends on the charge number Z as expected, but depends weakly on the

mass number. Indeed the impurity mass only impacts the gyro-bounce-averaging operator, where the Larmor radius and the banana width are proportional to \sqrt{A}/Z (Eq.3). But this A -dependence of the gyro-bounce-averaging operator is weak and does not depend on the sign of ω_r and the nature of the instability. Regarding the A -dependence, the impurity flux is expected to decrease as A increases, in both TEM and TIM cases. These results are in agreement with the numerical simulations.

This expression (Eq.22) can be further evaluated and we now consider the two different cases. The real frequencies $\omega_{r,n}$ and the linear growth rates γ_n are needed and determined by solving the linear dispersion relation (Eq.7). The saturation level of the plasma potential is given by nonlinear simulations.

A. Trapped electron mode case

For TEM instabilities, $\frac{\omega_{r,n}}{n} < 0$, therefore $(\frac{\omega_{r,n}}{n} - \frac{\Omega_d}{Z}E)$ is always negative. We evaluate the integral $\Gamma_{\psi,TEM}$ using Eq.(22), and we compare the results $D_{QLTEM} = -\Gamma_{\psi,TEM}/\partial_{\psi}n$ with those given by the nonlinear simulations (Fig.4).

As we focus on the Z dependance, we adjust the choice of $|\phi_n| = 0.05$ to get the best reasonable agreement between the two curves, but it should be noted that this choice is in qualitative agreement with the amplitude of the modes given by the nonlinear TERESA simulations. The results are presented in Fig.9. The dotted line corresponds to the nonlinear results already presented in Fig.4, and the solid line is D_{QLTEM} . As expected the quasi-linear diffusion coefficient is found to increase as a function of the impurity charge number. Here the quasi-linear flux is evaluated by summing over the n components of the Fourier decomposition in α . But it should be noted that the quasi-linear calculations yield almost the same results for Γ_{ψ} whatever the method we used: taking into account only the most unstable mode, or considering the sum over all unstable modes.

We remark that in that case there is a very good agreement between the quasi-linear theory and the results of the numerical simulations, despite the strong assumptions made in the quasi-linear calculations.

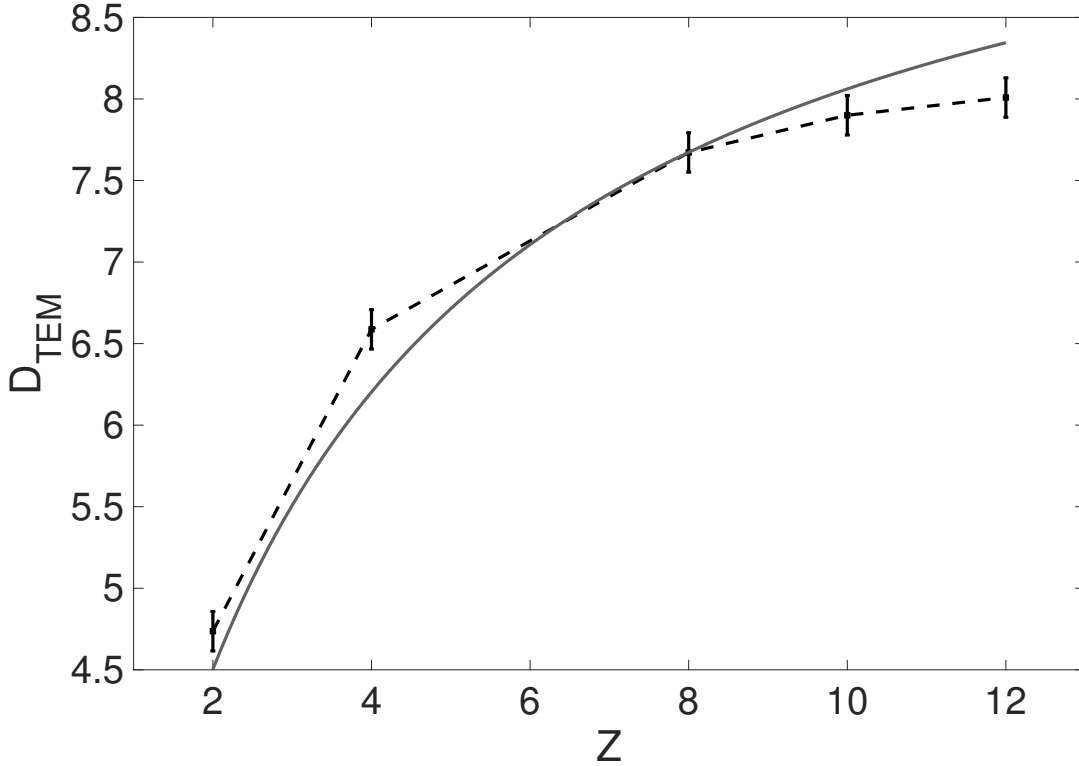


FIG. 9: Impurity diffusion coefficient D_{TEM} plotted against the impurity charge number Z in the case of TEM turbulence. The dotted line corresponds to the nonlinear results already presented in Fig. 4, and the solid line is D_{QLTEM} . As in the numerical simulations the quasi-linear diffusion coefficient is also found to increase as a function of the impurity charge number.

B. Trapped ion mode case

For TIM instabilities, $\frac{\omega_{r,n}}{n} > 0$, therefore resonance is possible, and by assuming γ_n small enough, the Lorentzian can be approximated in the resonant portion by:

$$\frac{\gamma_n}{(\omega_{r,n} - n\frac{\Omega_d}{Z}E)^2 + \gamma_n^2} \sim \pi\delta\left(\omega_{r,n} - n\frac{\Omega_d}{Z}E\right) \quad (23)$$

The integration over energy yields:

$$\Gamma_{\psi,TIM} = -\kappa_n \frac{n_0}{T_0^{3/2}} \sum_n |n\mathcal{J}\phi_n|^2 \pi \left(\frac{Z}{n\Omega_d}\right)^{3/2} \omega_{r,n}^{1/2} e^{-\frac{Z\omega_{r,n}}{n\Omega_d T_0}} \quad (24)$$

It should be noted that even though the delta-function expansion condition $\gamma_n/\omega_{r,n} \ll 1$ does not apply well in this case ($\gamma_n/\omega_{r,n} = 0.41$ for the most unstable mode), the monotonically decreasing dependence on Z is still captured by Eq.(24).

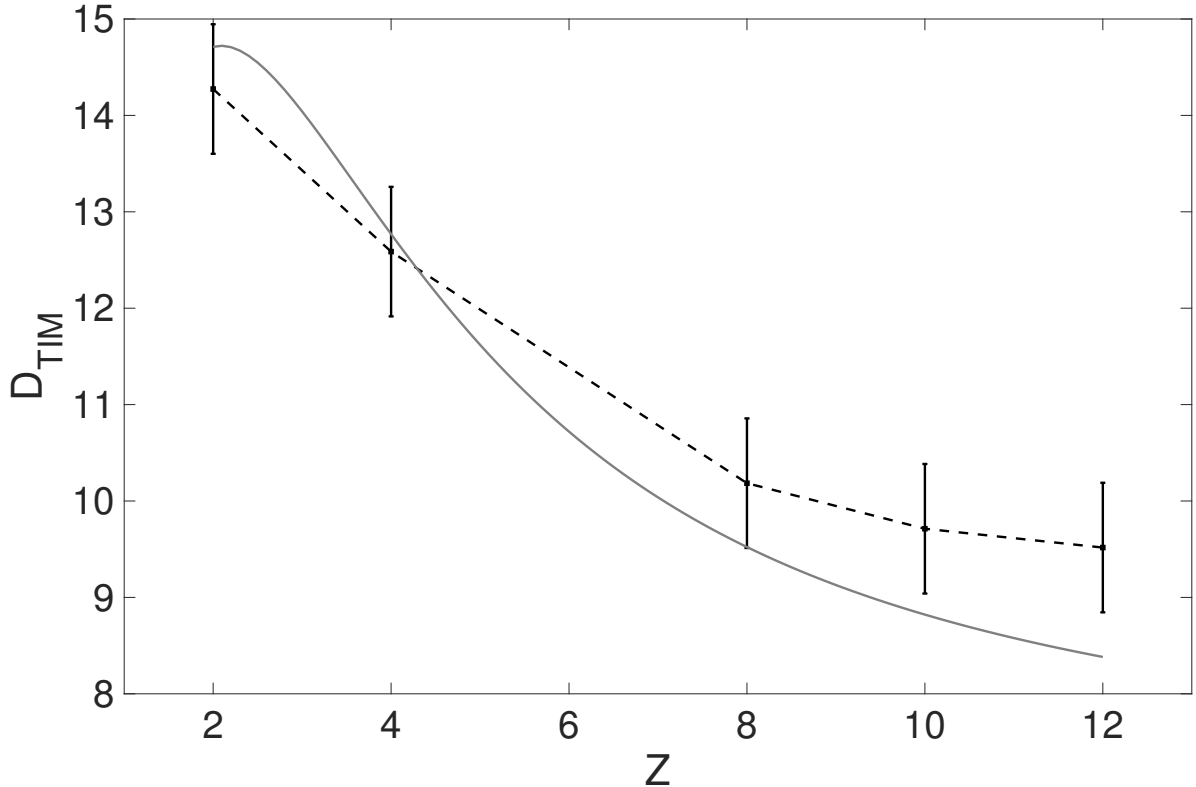


FIG. 10: Impurity diffusion coefficient D_{TIM} plotted against the impurity charge number Z in the case of TIM turbulence. The dotted line corresponds to the nonlinear results already presented in Fig. 7, and the solid line is D_{QLTIM} . The quasi-linear diffusion coefficient is also found to decrease as a function of the impurity charge number, the nonlinear flux and the quasi-linear prediction are in qualitative agreement.

But in order to limit the sources of discrepancies we evaluate numerically the quasilinear diffusion coefficients $D_{QLTIM} = -\Gamma_{\psi,TIM}/\partial_{\psi}n$ using Eq.(22) for $\Gamma_{\psi,TIM}$ and compare them with those given by the nonlinear simulations (Fig.7). In this case, to avoid small values of $\gamma_n/\omega_{r,n}$ only the most unstable mode $n = 60$ is retained in the calculation. The results are presented in Fig.10. The dotted line corresponds to the nonlinear results already presented in Fig.7, and the solid line is D_{QLTIM} . The quasi-linear diffusion coefficient is monotonically decreasing as a function of the impurity charge number, and the nonlinear flux and the quasi-linear prediction are in qualitative agreement. The maximum discrepancy is about equal to 15%. This result is not totally surprising considering the fact that nonlinear simulations and quasi-linear predictions are not always similar [34] for the TERESA model.

For the study presented in this article we can therefore conclude that both trends of

turbulent impurity transport with increasing Z (increasing in the TEM case and decreasing in the TIM case) are consistent with quasi-linear theory.

IV. CONCLUSION

In the present article the impact of the charge and mass numbers on impurity turbulent fluxes has been investigated via both gyro-bounce-kinetic simulations and quasi-linear theory. All the results shown in this work are from simulations and calculations carried out with the TERESA model. The trapped particles are treated kinetically, while the passing particles respond adiabatically. The model is meant to investigate fundamental mechanisms and trends, rather than provide realistic quantitative predictions for tokamaks. The simulation parameters correspond to a radial box size of 166 Deuterium Larmor radii.

While impurity transport depends weakly on the impurity mass, it is found that it is mainly dependent on the impurity charge number. Moreover, it is found that impurity transport depends on the background turbulence: Impurity flux due to TEM turbulence increases with Z while it decreases with Z in the case of TIM turbulence. In contrast, for the A -dependence we observe that the diffusion coefficient decreases weakly with increasing A in both TEM and TIM cases.

The methodology of quasi-linear theory has been shown to be applicable in this case as it determines the relative strength of the impurity ion transport and qualitatively explains the results given by the nonlinear numerical simulations.

Acknowledgments

This work has been carried out within the framework of the French Federation for Magnetic Fusion Studies (FR-FCM) and of the Eurofusion consortium, and has received funding from the Euratom research and training programme 2014-2018 and 2019-2020 under grant agreement No 633053. The views and opinions expressed herein do not necessarily reflect those of the European Commission.

This work was granted access to the HPC resources of IDRIS under the allocation 2017-27862 made by GENCI (Grand Equipement National de Calcul Intensif).

-
- [1] T. Putterich, R. Neu, R. Dux, A.D. Whiteford, M.G. O'Mullane, H.P. Summers and the ASDEX Upgrade Team, Nucl. Fusion 50, 025012 (2010)
- [2] C. Angioni, R. Bilato, F. J. Casson, E. Fable, P. Mantica, T. Odstrcil, M. Valisa, ASDEX Upgrade Team and JET Contributors, Nucl. Fusion 57 022009 (2017)
- [3] W. Guo, L. Wang, G. Zhuang, Phys. Plasmas 23, 112301 (2016)
- [4] H. Nordman, A. Skyman, P. Strand, C. Giroud, F. Jenko, F. Merz, V. Naulin, T. Tala and the JET-EFDA Contributors, Plasma Phys. Cont. Fusion 53, 105005 (2011)
- [5] H. Du, Z. X. Wang, J. Q. Dong, S. F. Liu, Phys. Plasmas 21, 052101 (2014)
- [6] N. Bonanomi, P. Mantica, C. Giroud, C. Angioni, P. Manas, S. Menmuir, and JET Contributors, Nucl. Fusion 58, 036009 (2018)
- [7] S. Futatani, W. Horton, S. Benkadda, I. O. Bespamyatnov, and W. L. Rowan, Phys. Plasmas 17, 072512 (2010)
- [8] C. Angioni, R.M. McDermott, E. Fable, R. Fischer, T. Putterich, F. Ryter, G. Tardini, and the ASDEX Upgrade Team. Nucl. Fusion 5, 023006 (2011)
- [9] F. J. Casson, C. Angioni, E. A. Belli, R. Bilato, P. Mantica, T. Odstrcil, T. Putterich, M. Valisa, L. Garzotti, C. Giroud et al., Plasma Phys. Cont. Fusion 57, 014031 (2015)
- [10] T. Fulop and H. Nordman, Phys. Plasmas 16, 032306 (2009)
- [11] A. Skyman, L. Fazendeiro, D. Tegnered, H. Nordman, J. Anderson, and P. Strand, Nucl. Fusion 54, 013009 (2014)
- [12] Y. Camenen, A. G. Peeters, C. Angioni, F. J. Casson, W. A. Hornsby, A. P. Snodin, and D. Srintzi, Phys. Plasmas 16, 012503 (2009)
- [13] P. Manas, W. A. Hornsby, C. Angioni, Y. Camenen, and A. G. Peeters, Plasma Phys. Cont. Fusion 59, 035002 (2017)
- [14] M. Idouakass, E. Gravier, M. Lesur, J. Médina, T. Réveill e, T. Drouot, X. Garbet and Y. Sarazin, Phys. Plasmas 25, 062307 (2018)
- [15] T. Drouot, E. Gravier, T. Reveille, A. Ghizzo, P. Bertrand, X. Garbet, Y. Sarazin and T. Cartier-Michaud, Eur. Phys. Journal D 68, 280 (2014)
- [16] F. Jenko, T. Dannert, C. Angioni, Plasma Phys. Cont. Fusion 47, B195 (2005)
- [17] C. Bourdelle, J. Citrin, B. Baiocchi, A. Casati, P. Cottier, X. Garbet, F. Imbeaux and JET Contributors, Plasma Phys. Cont. Fusion 58, 014036 (2016)

- [18] M. Tagger, G. Laval, and R. Pellat, *Nucl. Fusion* 17, 109 (1977)
- [19] H. Biglari, P. H. Diamond, and P. W. Terry, *Phys. Fluids* 31, 2644 (1988)
- [20] G. Depret, X. Garbet, P. Bertrand, A. Ghizzo, *Plasma Phys. Cont. Fusion* 42, 949 (2000)
- [21] Y. Sarazin, V. Grandgirard, E. Fleurence, X. Garbet, Ph. Ghendrih, P. Bertrand and G. Depret, *Plasma Phys. Control. Fusion* 47, 1817 (2005)
- [22] T. Drouot, E. Gravier, T. Reveille, M. Sarrat, M. Collard, P. Bertrand, T. Cartier-Michaud, P. Ghendrih, Y. Sarazin and X. Garbet, *Phys. Plasmas* 22, 082302 (2015)
- [23] T. Drouot, E. Gravier, T. Reveille, M. Collard, *Phys. Plasmas* 22, 102309 (2015)
- [24] T. Cartier-Michaud, P. Ghendrih, V. Grandgirard, and G. Latu, *ESAIM: Proc.* **43**, 274 (2013)
- [25] T. Cartier-Michaud, P. Ghendrih, Y. Sarazin, G. Dif-Pradalier, T. Drouot, D. Estève, X. Garbet, V. Grandgirard, G. Latu, C. Norscini, C. Passeron, *J. Phys.: Conf. Series* 561, 012003 (2014)
- [26] A. Ghizzo, D. Del Sarto, X. Garbet, Y. Sarazin, *Phys. Plasmas* 17, 092501 (2010)
- [27] E. Gravier, M. Lesur, T. Reveille, T. Drouot, *Phys. Plasmas* 23, 092507 (2016)
- [28] E. Gravier, M. Lesur, T. Reveille, T. Drouot, J. Médina, *Nucl. Fusion* 57 124001 (2017)
- [29] B. Kadomtsev, O.P. Pogutse, *Reviews of Plasma Physics*, Consultants Bureau, New-York, 5:249 (1970)
- [30] X. Garbet, Y. Idomura, L. Villard and T.H. Watanabe, Gyrokinetic simulations of turbulent transport, *Nucl. Fusion* 50, 043002 (2010)
- [31] J. C. Lagarias, J. A. Reeds, M. H. Wright and P. E. Wright, *SIAM J. Optimization* 9, 112 (1998)
- [32] E. Sonnendrücker, J. Roche, P. Bertrand and A. Ghizzo, *Journ. Comp. Phys.* 149, 201 (1999)
- [33] M. Lesur, T. Cartier-Michaud, T. Drouot, P. H. Diamond, Y. Kosuga, T. Reveille, E. Gravier, X. Garbet, S.-I. Itoh and K. Itoh, *Phys. Plasmas* 24, 012511 (2017)
- [34] J. Médina, M. Lesur, E. Gravier, T. Reveille, M. Idouakass, T. Drouot, P. Bertrand, T. Cartier-Michaud, X. Garbet and P. H. Diamond, *Phys. Plasmas* 25, 122304 (2018)